Vietnam Journal of Marine Science and Technology 2026, 26(1) 1–19

Vietnam Academy of Science and Technology

Vietnam Journal of Marine Science and Technology

journal homepage: vjs.ac.vn/index.php/jmst

Numerical simulation of seasonal currents in the Mekong Coastal Area: a case in 2019

Nguyen Thanh Duong, Vu Duy Vinh*, Nguyen Minh Hai

Institute of Science and Technology for Energy and Environment, VAST, Vietnam

Received: 10 January 2025; Accepted: 6 April 2025

ABSTRACT

This study employing the Delft3D numerical model investigated the Mekong Delta's seasonal current dynamics, simulating its hydrodynamic regime in 2019. Using Nash-Sutcliffe Efficiency and Root Mean Square Error metrics, the model's accuracy in replicating measured water levels (cm) and currents at various stations was validated, achieving acceptable simulation results. This allowed for reliable analysis of the delta's current patterns. The study revealed that while the overall direction and peak velocity of current remain relatively consistent throughout the year, their spatial distribution undergoes significant shifts, particularly during the transitional periods between seasons. Monthly flow velocities reflect this seasonality, with strong (up to 1 m/s) and consistent northeast-southwest surface flows during the low flow season (minimal stratification), driven by northeasterly winds. Conversely, the flood season exhibits greater regional variability in velocity and direction due to strong freshwater input and fluctuating winds, with surface velocities reaching 1 m/s in the Mekong estuary in October but decreasing sharply with depth (strong stratification), and flow directions shifting dynamically throughout the season.

Keywords: Seasonal currents, Mekong, Delft3D, hydrodynamics, modeling.

*Corresponding author at: Institute of Science and Technology for Energy and Environment, 18 Hoang Quoc Viet Street, Nghia Do Ward, Hanoi, Vietnam. *E-mail addresses*: vinhimer@gmail.com

https://doi.org/10.15625/1859-3097/22266

Introduction

The Mekong River Delta (MRD), a vital socio-economic and ecological resource in Southeast Asia, faces unprecedented environmental challenges. This mixed-energy delta, crucial for Vietnam's rice and seafood exports, is shaped by a complex interplay of river discharge, tidal forces from the East Sea (ES) and Gulf of Thailand (GoT), and monsoon-driven coastal currents [1–3]. Understanding the seasonal variability of these currents is paramount for predicting and managing the delta's response to both natural and anthropogenic pressures. This mixed-energy delta, essential for Vietnam's rice and seafood exports, is facing an unprecedented crisis driven by the drastic reduction of sediment flux due to rapid upstream dam construction and intensive in-delta sand mining. This sediment deficit is a primary driver of land subsidence (0.1–81 cm/decade) and sea-level rise (2–3 mm/year), resulting in alarming annual land loss (300–500 hectares) [4, 5]. The seasonal patterns of currents play a crucial role in the distribution of this reduced sediment load, influencing erosion, accretion, and the overall stability of the delta.

From a hydrodynamic perspective, the seasonal variations in ocean currents, with their significant spatial and temporal variability, govern water exchange and material transport, directly impacting ecological conditions such as nutrient dispersal and primary productivity [4, 6]. The complex interaction between river flow, tides, and monsoon winds generates highly variable current patterns across the MRD [1–5]. Unverricht et al. [6] highlighted the role of tidal resuspension mechanisms in shaping land-ocean interactions during inter-monsoon seasons, emphasizing the direct link between hydrodynamics and sediment dynamics, which are fundamentally driven by current patterns. Dang et al. [7] used satellite imagery to reveal strong links between observed data of Mekong floodplains and regional management strategies, underlining the importance of understanding hydrodynamic processes for effective delta management.

Previous studies have explored MRD hydrodynamics. Tien [8] utilized the MIKE 21/3 COUPLE model to analyse hydrodynamic and wave processes during storm events, emphasizing land-sea interactions and their impact on erosion and sedimentation. Tanh et al. [10] focused on eddy currents in the Vam Nao River using 2D and 3D simulations, revealing recirculating flows. However, these studies primarily relied on water level calibration, potentially limiting the accuracy of current simulations. Dang et al. [11] evaluates the impacts of hydropower dams and flood prevention systems on the hydrological regimes of the Mekong floodplains, known for their agricultural productivity and biodiversity, through a systematic analysis of indicators of hydrological alterations and flood extent observations till 2013. Vinh et al. [4] focusing mostly on the sediment dynamics due to seasonal forcing in Mekong coastal area using Delft3D, leaving the detailed seasonal variation of currents in the MRD largely unexplored.

In this study, we leverage the Delft3D numerical modelling framework to comprehensively investigate seasonal current variations in the MRD, focusing on the interplay between river discharge and monsoon wind conditions. By conducting rigorous simulations and sensitivity analyses, incorporating tidally induced effects near major outlets, we aim to quantify the seasonal variations in current magnitude and direction. This research provides crucial insights into the seasonal variability of current patterns, enabling more informed predictions of sediment transport, salinity intrusion, and ecosystem responses, ultimately benefiting stakeholders including policymakers, engineers, and scientists engaged in sustainable management.

Materials and methods

Over the past ~8,000 years, the Mekong Delta has prograded southwestward into the East Sea (ES), forming the Ca Mau Peninsula on a wide (~250 km), gently sloping continental shelf. This asymmetrical growth has resulted in the delta's present shape, although some shoreline erosion has occurred, particularly along parts of the modern coast and the Ca Mau Peninsula. The

Mekong River itself splits into two main branches, the Tien (north) and Hau (south/Bassac), creating the "nine dragons"—its nine primary river mouths. The Tien branch has three main estuaries with multiple outlets, while the Hau has two. North of the MRD, the Dong Nai–Saigon River system also empties into the ES, with the Saigon River's Soai Rap branch receiving the Vamco River just before reaching the sea [12] (Fig. 1).

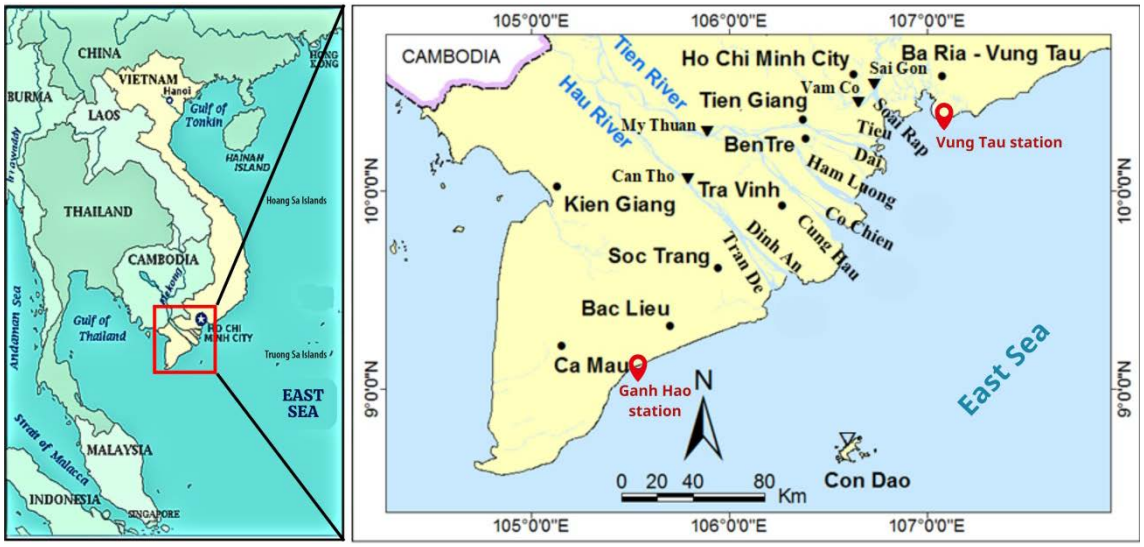

Figure 1. The MRD and its region of freshwater influence with locations of measurements (Vung Tau and Ganh Hao stations) [4]

The MRD has been experiencing rapid population growth, urbanization, increased river transportation, agricultural expansion (at the expense of forests), and booming aquaculture, combined with mangrove loss (partially offset by replanting), intensifying fishing and oil/gas activities, upstream damming, and climate change, creates significant environmental risks.

The Mekong River basin experiences a tropical climate with two main seasons: the wet season (June to October) and the dry season (November to May). The wet season, driven by the Southwest monsoon, brings 85–90% of the year's rainfall. These seasonal monsoons also affect the ocean, influencing winds, waves, and how the river's freshwater mixes with the ocean's salt water, impacting sediment movement. Specifically, off the Bassac River in South Vietnam, the Southwest monsoon brings lighter winds and slow, northeast-flowing currents, while the Northeast monsoon brings strong winds, increased wave action that stirs up seabed sediment, and southwest-flowing coastal currents. Overall rainfall in South Vietnam ranges from 1,600 to 2,400 mm annually, with the western region receiving the most and the central delta the least [1, 12].

The Mekong River discharges about 500 $km^3.yr^{-1}$, with most (85%) flowing during the flood season (September to November) and the rest (15%) during the low flow season (December to August) [13].

In the Mekong River Delta, flooding occurs after the local rainy season because the water comes mainly from upstream and is influenced by the Tonle Sap Lake in Cambodia. Coastal currents in the MRD change their direction with the monsoon seasons, flowing southwest during the winter monsoon and northeast during the summer monsoon [14].

Tides play a crucial role in how water is distributed in deltas and how sediment moves in estuaries [15, 16]. In the central and lower parts of estuaries, sediment buildup is largely controlled by the turbidity maximum zone, which are formed and changed due to the interaction between river flow and tidal movement, including

processes like tidal pumping and density differences [12, 17, 18].

The MRD experiences a mix of diurnal and semi-diurnal tides. The main semi-diurnal tides (M2 and S2) have amplitudes up to 0.9 and 0.5 m, respectively, while the main diurnal tides (K1 and O1) reach up to 0.7 and 0.5 m [15]. Overall tide height decreases along the delta, from a maximum of 3.8 m in the Northeast to around 2 meters in the Southwest along the Ca Mau peninsula [19]. The tides near the Mekong's mouth rise and fall about 3.5 m during high (spring) tides. This tidal range decreases as going upriver: about 2 m at Can Tho (90 km upstream) and about 1 m at 190 km upstream [20].

Materials

For model setup

Coastline and water depth information for the MRD's coastal area were taken from detailed maps (scales 1:50,000 and 1:25,000) created in Vietnam's national VN2000 coordinate system (which is similar to a standard UTM projection) and published in 2019 by Vietnam's Ministry of Natural Resources and Environment. The deeper, offshore water depth data were taken from the GEBCO-1/8 dataset, which provides a global grid of ocean depths at roughly 30 arc-second intervals [21].

To model the rivers, water flows measured at My Thuan (Tien River) and Can Tho (Hau River) from 2013 to 2023 were used. Due to there were no measuring stations on the Vamco and Soai Rap Rivers (north of the Mekong River Delta), average river discharge for low and flood seasons from a previous study [21] were used for these rivers.

Wind and wave data at Con Dao Island and Vung Tau (2020–2023) were exploited. To model surface conditions in the area, meteorological data (wind, air temperature, humidity, cloud cover, rainfall, evaporation-precipitation, and mean sea level pressure) was obtained every six hours from the ECMWF Re-analysis-5 (ERA5) dataset, which has a spatial resolution of $0.125^{o} \times 0.125^{o}$. This ERA5 data was used to define the model's open boundary conditions [4].

For model calibration and validation

To ensure accuracy, the model was calibrated and validated using water level and current measurements at Vung Tau and Ganh Hao stations, respectively of the project "Interaction between hydrodynamics of the East Sea and Mekong River water" (Fig. 1). Tidal patterns were determined by analyzing nearshore sea level measurements to extract harmonic constants for eight main tidal constituents (M2, S2, K2, N2, O1, K1, P1, and Q1). These constants, along with offshore tidal harmonic data from the FES2022 database, were used to define tidal conditions at the model's sea boundaries. For broader ocean transport conditions in the initial (parent) model, data from the World Ocean Atlas (with a 0.25o grid resolution) was used [4].

Methods

The Delft3D model

This study used two modules of Delft3D, Delft3D-Flow and Delft3D-Wave, to simulate water movement (tides, currents, and waves) and the movement of suspended sediment. Delft3D-Flow, developed by Deltares, is a 3D model designed to study water flow, sediment transport, changes in landforms, and water quality in rivers, estuaries, and coastal areas. It uses complex mathematical equations (Reynolds-averaged Navier-Stokes equations) and a specific method (k-ε turbulence closure model) to calculate water movement, using a grid system that adapts to the shape of the area being studied [22].

The Delft3D-Wave model is based on SWAN, a dedicated wave model. SWAN calculates wave behaviour using an equation that balances wave energy. This study used specific settings within SWAN: the JONSWAP expression was used to calculate friction at the seabed, with a specific value (C_{jon} = 0.067 $m^2.s^{-3}$) for shallow water conditions [22]. Additionally, the model by Battjes and Janssen [23] was used to simulate how waves lose energy as they break in shallow water.

Model setup

The model uses a curvilinear grid, which allows for higher resolution in key areas and lower resolution elsewhere. This grid covers the entire coastal zone from Binh Thuan coastal area (Vietnam) to Preah Sihanouk (Cambodia) (Fig. 2) (a distance of approximately 500 km along the coast and 180 km offshore), using a grid of 890 by 361 nodes with varying grid sizes (from 23.6 m to 3,912.2 m). Vertically, the model grid uses four layers in a sigma coordinate system, consistents with the parent model. This hydrodynamic model accounts for the effects of water temperature, salinity, and wave action.

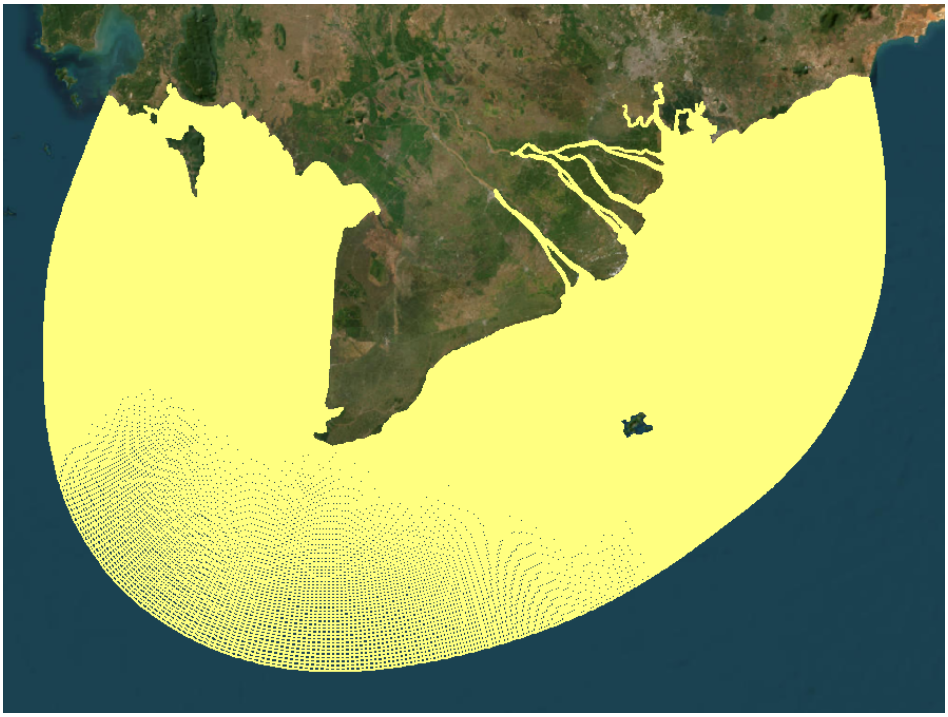

Figure 2. The grid of the study area

The model was created and run with very short time step of 0.2 minutes (12 seconds) to simulate river flow. To ensure the model's accuracy, it was calibrated and validated using data from four distinct periods: Northeast monsoon (dry season - January), transition season (May), Southwest monsoon (July), and flood season (October). These periods represent different flow conditions, allowing for a comprehensive evaluation of the model's performance.

The model included four open river boundaries: Soai Rap, Vamco, My Thuan, and Can Tho. The Soai Rap and Vamco boundaries are part of the Dong Nai–Saigon River system. Hourly water discharge measurements from Can Tho and My Thuan were used as input data (boundary conditions). For the other two boundaries, constant flow rates were used: 546.9 $m^3.s^{-1}$ (Soai Rap) and 52.5 $m^3.s^{-1}$ (Vamco) during low flow, and 1,310 $m^3.s^{-1}$ (Soai Rap) and 177.8 $m^3.s^{-1}$ (Vamco) during flood season [1, 4].

For other conditions, average water temperature (27.5°C in the low flow season and 27.2°C in the flood season) and zero salinity were set at the river boundaries. Wind data, including speed and direction, recorded every six hours at Con Dao from 2020 to 2023, was also incorporated into the model. Additionally, a wave module was directly linked to the hydrodynamics, with wave conditions at the sea boundary derived from existing wave climate data [4].

Bottom friction was represented using Manning's (n) coefficients, ranging from 0.018 to 0.023 $m^{-1/3}$.s [23]. After calibration, both background horizontal eddy viscosity and diffusivity were set to 8 $m.s^{-2}$. To account for smaller-scale turbulence, the Horizontal Large Eddy Simulation (HLES) sub-grid model, based on the work of Uittenbogaard and Van Vossen, was used within the Delft3D-Flow model [22]. This HLES model added calculated values to the background viscosity and diffusivity to better represent turbulent mixing.

Calibration and validation process

To ensure the model's accuracy, it was tested against real-world data from different flow conditions. This involved simulating the low flow and flood seasons of 2019 and 2020. The accuracy of each simulation was evaluated by comparing the model's results to actual measurements using the Nash-Sutcliffe efficiency (*NSE*) metric [24], calculated as follows:

$$NSE = 1 - \frac{\sum_{i=1}^{n}\left(Y_i^{obs} - Y_i^{sim}\right)^2}{\sum_{i=1}^{n}\left(Y_i^{obs} - Y^{mean}\right)^2} \quad (1)$$

where: Y_i^{obs} is the ith observation for the constituent being evaluated, Y_i^{sim} is the ith simulated value for the constituent being evaluated, Y^{mean} is the mean of observed data for the constituent being evaluated, and n is the total number of observations.

Root Mean Square Error (*RMSE*) is a widely used metric for quantifying the difference between simulated and observed data. Essentially, the RMSE measures the average magnitude of the errors between two datasets by comparing observed (or known) values with predicted values. A lower RMSE indicates a better fit between the simulated and observed data, while a higher *RMSE* signifies a greater discrepancy [25]:

$$RMSE = \sqrt{\frac{\sum_{i=1}^{n} X_{obs,i} - X_{sim,i}}{n}} \# \quad (2)$$

where: $X_{obs,i}$, $X_{sim,i}$ are ith observational, simulated values; n is the total number of observations.

Results and disscusion

Model validation from field measurements

To ensure the accuracy and reliability of the hydrodynamic model, we employed a rigorous calibration and validation process using both simulated and measured water levels in Vung Tau station in 2019, for both calibration (specifically determining the Manning coefficient) and validation (Table 1, Fig. 3). After calibration, the model's water level predictions closely matched the measurements, with *NSE* values ranging from 0.834 to 0.976 and *RMSE* values ranging from 0.126 to 0.331, indicating an acceptable simulation.

Table 1. NSE and *RMSE* values of measured and simulated water level (m) in Vung Tau station

Efficiency / Time	*NSE*	*RMSE*
January 2019	0.834	0.331
May 2019	0.976	0.126
July 2019	0.955	0.186
October 2019	0.887	0.277

While most tidal days experience two high and two low tides, during neap tide periods when the difference between high and low tides is at its minimum—a distinct phenomenon can occur: a single tide. This single tide is characterized by just one high water and one low water within a tidal day, and we will refer to these as single high water and single low water, respectively. These single tides manifest in two different forms, likely referring to variations in their overall shape or duration. They appear twice within a synodic month (the period of the Moon's phases, approximately 29.5 days), with an average recurrence period of 13.66 days. This means that roughly every two weeks, during the neap tide phase, a location might experience this single high and single low water pattern instead of the typical double tide cycle.

The comparison between simulated and measured currents in 2019 revealed an acceptable agreement after calibration (Fig. 4, Table 2). This close correspondence is quantitatively demonstrated by the *NSE* values, which ranged from above 0.7 to over 0.8. These

high *NSE* values indicate that the model effectively captures the variance in the observed data and provides a good representation of the temporal dynamics of the currents. Furthermore, the *RMSE* values, ranging from 0.054 to 0.073 m/s, further corroborate the model's accuracy. These relatively low *RMSE* values suggest a minimal average difference between the simulated and measured current speeds, highlighting the model's ability to relatively accurately predict current magnitudes. The regular fluctuation of the efficiency values throughout the simulation period indicates a consistent and acceptable level of performance, demonstrating the model's robustness and its ability to maintain accuracy under varying conditions. This consistent performance strengthens the confidence in the model's ability to provide reliable predictions of currents in the Ganh Hao region.

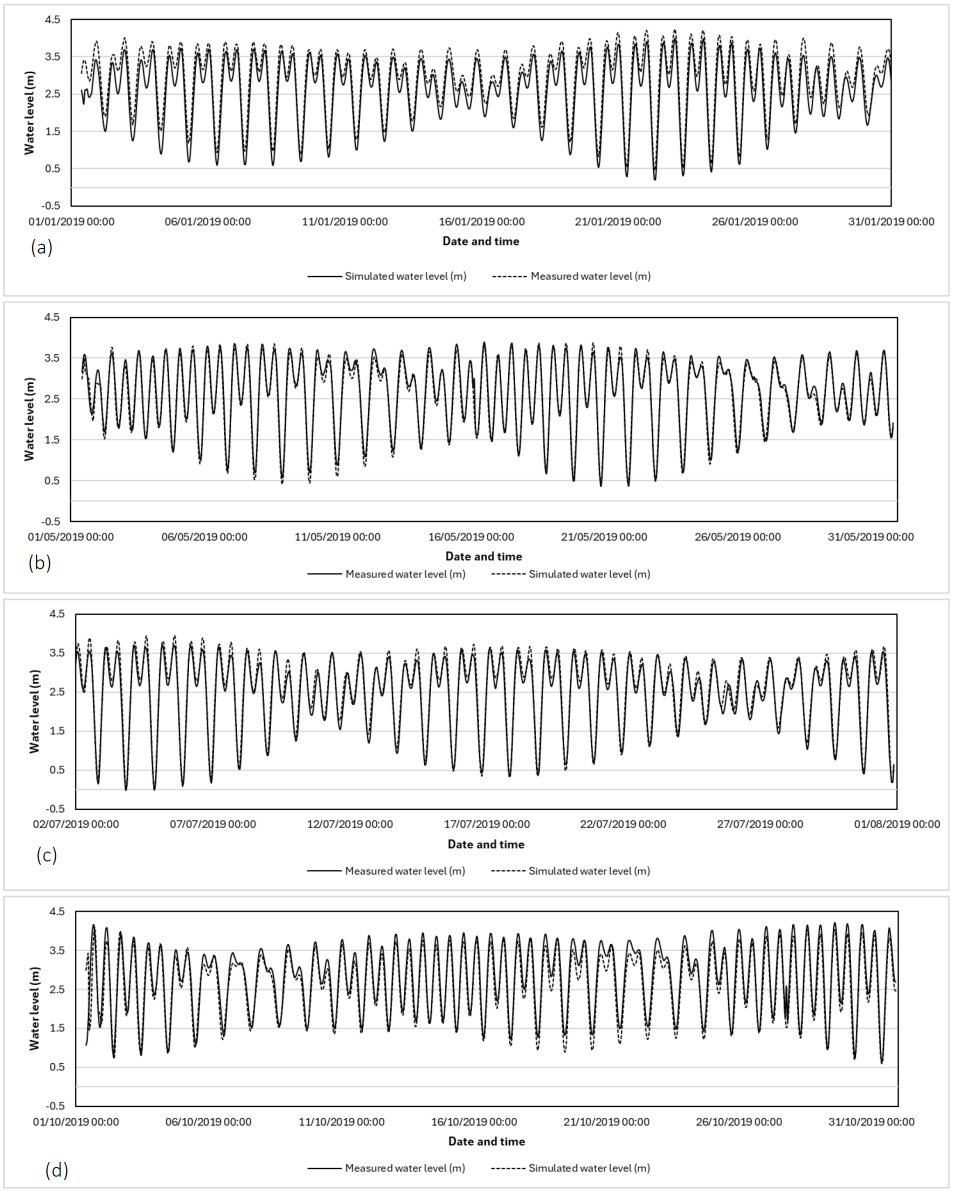

Figure 3. Comparison between simulations and measurements of water level in Vung Tau station in January (a), May (b), July (c) and October (d) 2019

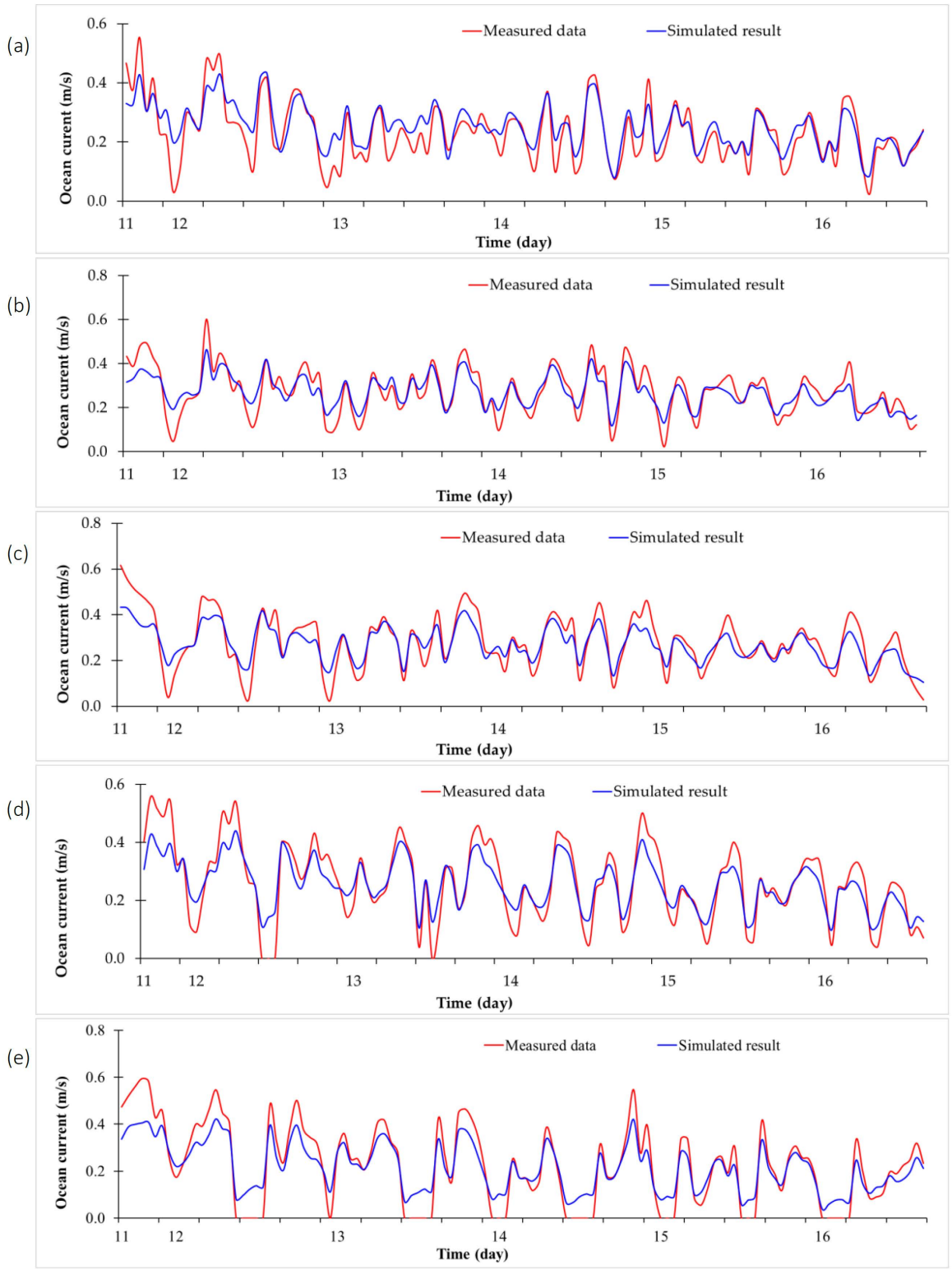

Figure 4. Comparison between simulations and measurements of current speed throughout a water column in Ganh Hao station in February 2019 (a–e: from surface to bottom layers)

Table 2. NSE and *RMSE* values of measured and simulated current (m/s) throughout a water column in 2019 in Ganh Hao station

Efficiency / Layer	*NSE*	*RMSE*
1	0.722	0.054
2	0.751	0.054
3	0.754	0.059
4	0.79	0.061
5	0.815	0.073

Northeast monsoon (Dry season)

In January, during the Northeast monsoon with reduced rainfall, tidal currents dominate the MRD's hydrodynamics. Surface currents vary significantly, ranging from 0.05 to 1 m/s. The strongest currents (0.65–1 m/s) are concentrated within the rivers and estuaries, indicating a strong riverine influence on water flow (Fig. 5). Outside these areas, surface currents are considerably weaker. Notably, the direction of these currents diverges significantly, with a general southward movement from the north and a prevailing southwestward to westward flow.

During flood tides (Figs. 5a, b), currents exhibit distinct vertical stratification. Near the coast, surface currents reach speeds of up to 1 m/s, while bottom currents are slower, around 0.7 m/s. The highest velocities are observed in the southern part of the study area. A sharp decrease in current velocity occurs from the surface to the bottom layers, with bottom currents outside the estuaries dropping below 0.2 m/s. However, within the rivers themselves, bottom current velocities remain relatively high, highlighting the confined nature of the river channels and their influence on flow dynamics.

Ebb tides (Figs. 5e, f) present a different scenario, characterized by rapid river discharge into the ocean, with current speeds reaching 1 m/s throughout the water column. Coastal currents also remain strong during ebb tide, peaking at 1 m/s at the surface and 0.7 m/s at the bottom. Offshore surface currents range from 0.4 to 0.8 m/s, reflecting the outflow of water from the delta. In stark contrast, bottom currents offshore are extremely weak, measuring less than 0.05 m/s. This signifies that the ebb tide's influence is primarily confined to the surface and near-coastal regions, with minimal impact on deeper offshore waters.

Transition season

It is marked a significant shift in current patterns compared to previous months, coinciding with the transition from the northeast to southwest monsoon and increased rainfall. A clear divergence in current direction persists, with surface currents varying considerably between 0.05 and 1 m/s. The strongest currents (0.65–1 m/s) are concentrated within rivers and estuaries, while areas outside these channels experience significantly weaker currents. Notably, the current direction also diverges, generally flowing southward in the north and southwestward to westward elsewhere. This suggests a complex interplay of riverine discharge and coastal processes influencing water movement during this transitional period (Fig. 6).

During ebb tides (Figs. 6e, f), a distinct vertical stratification of currents is observed. Surface currents can reach speeds of up to 1 m/s across much of the study area, but bottom currents are generally slower. In rivers and estuaries, bottom currents range from 0.8 to 1 m/s, while in other areas they measure between 0.2 and 0.5 m/s. This sharp decrease in velocity from surface to bottom indicates a strong influence of bottom friction and potentially density stratification, hindering deeper water movement during ebb tides.

Flood tides (Figs. 6a, b) present a contrasting picture, characterized by rapid tidal currents flowing into the rivers, with current velocity reaching 1 m/s throughout the entire water column within these channels. Outside the estuaries, coastal currents maintain a relatively consistent speed, ranging from 0.3 to 0.7 m/s from surface to bottom. Offshore surface currents range from 0.1 to 0.8 m/s, with the lowest velocities concentrated in the central part of the study area. This suggests a more homogenous vertical current profile during flood tides, driven by the strong incoming tidal surge.

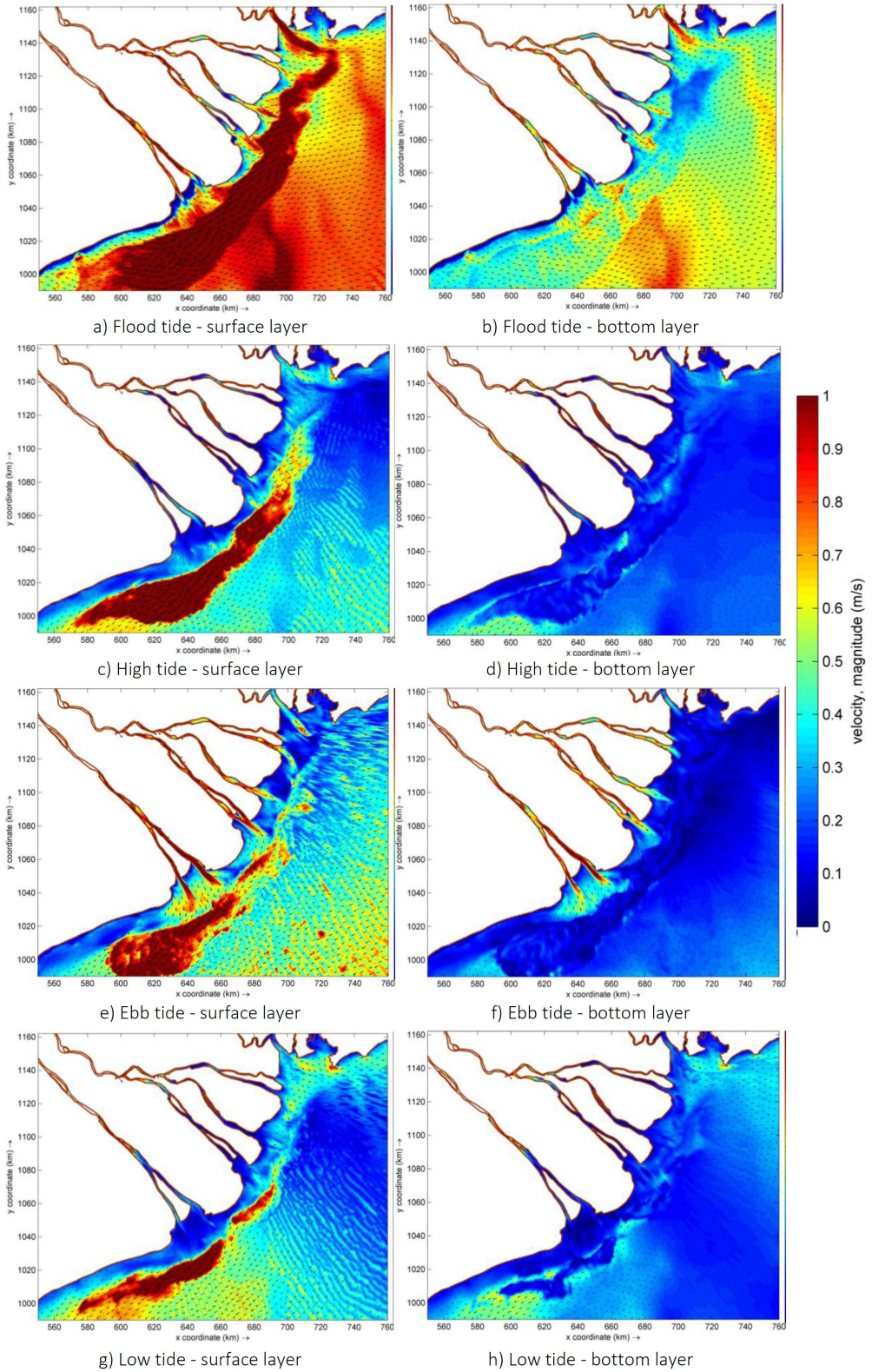

Figure 5. Current velocity (m/s) during the spring tide in January 2019

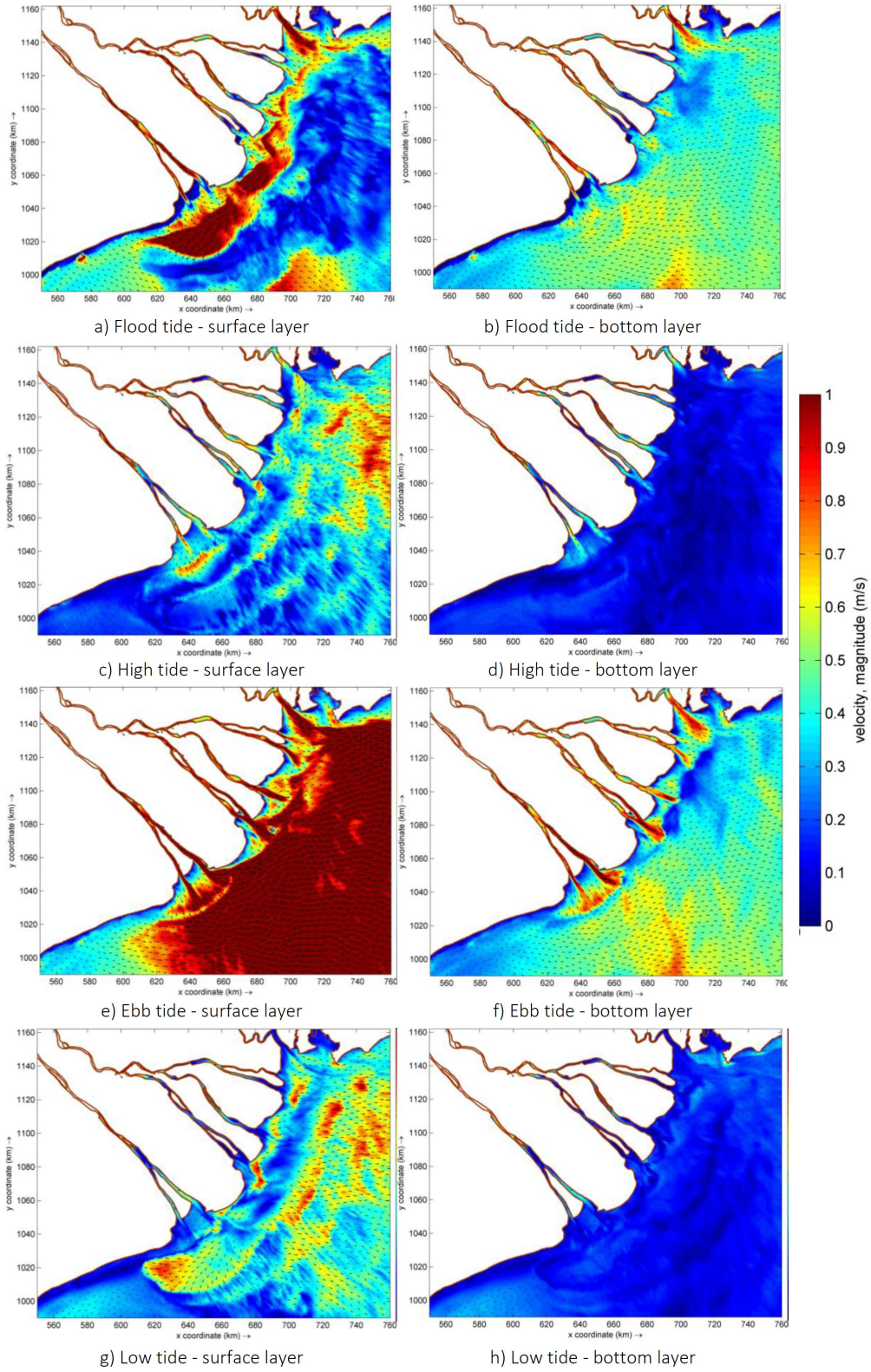

Figure 6. Current velocity during (m/s) the spring tide in May 2019

Southwest monsoon

The shift from May to July brings significant changes to surface currents, coinciding with peak rainfall and increased river flow during the Southwest monsoon. Current speeds vary widely, from 0.05 to 1 m/s. While the strongest currents (0.65–1 m/s) remain concentrated in rivers and estuaries, similar to the dry season, their velocities are slightly reduced. Outside these areas, surface currents weaken considerably, generally staying below 0.3 m/s. A key difference emerges in current direction: a general southward movement is observed in the north, transitioning to a predominantly southwestward to westward flow overall. This indicates a complex interplay of river discharge and coastal influences shaping the surface current patterns (Fig. 7).

Analyzing the vertical structure of currents during flood tides (Figs. 7a, b) reveals distinct stratification. Near the coast, surface currents reach up to 1 m/s, while bottom currents are slower, around 0.6 m/s, with the strongest velocities observed in the southern part of the study area. A sharp decrease in velocity occurs from surface to bottom, especially outside the estuaries where bottom currents fall below 0.4 m/s. However, within the rivers, bottom currents maintain relatively high speeds, exceeding 0.6 m/s. This suggests that during flood tides, the influence of tidal forcing is stronger at the surface and near the coast, while river flow maintains a stronger bottom current within the river channels.

Ebb tides (Figs. 7e, f) present a contrasting scenario, characterized by much faster river discharge into the ocean, with current speeds reaching 1 m/s throughout the water column. Coastal currents also remain strong, peaking at 1 m/s at the surface and ranging from 0.4 to 0.7 m/s at the bottom. Offshore surface currents, ranging from 0.4 to 0.8 m/s, reflect this delta outflow. Notably, the offshore bottom currents are extremely weak, measuring less than 0.05 m/s. This stark difference indicates that the ebb tide's influence is primarily confined to the surface and near-coastal regions, with minimal impact on deeper offshore waters, emphasizing the dominant role of river discharge during ebb tide.

Flood season

The transition from the wet season (July) to the flood season (October) witnesses a westward shift in the current ocean direction, with maximum speeds reaching 1 m/s. This westward trend and speed profile become similar to the current patterns observed during the full dry season. This shift coincides with decreasing rainfall and a growing dominance of tidal currents, suggesting a clear link between seasonal precipitation, tidal influence, and current patterns (Fig. 8).

Analysis of current stratification during flood tides (Figs. 8a, b) reveals distinct vertical differences. Surface currents near the coast and within the river channels can reach 1 m/s, while bottom currents are significantly slower, ranging from 0.4 to 0.6 m/s, with the highest bottom velocities observed in the southern region. A sharp decrease in velocity from the surface to the bottom is evident, especially outside the estuaries where bottom currents drop below 0.6 m/s. However, within the rivers themselves, bottom currents remain relatively strong, exceeding 0.7 m/s. This indicates that tidal forcing exerts a stronger influence on surface and near-coastal currents during flood tides, while river flow maintains stronger bottom currents within the river channels.

During ebb tides (Figs. 8e, f), a similar vertical stratification is observed, although the overall current speeds are higher due to increased river discharge into the ocean. Current speeds reach 1 m/s throughout the water column, with strong coastal currents also present (up to 1 m/s at the surface and 0.4 to 0.7 m/s at the bottom). Offshore surface currents, ranging from 0.4 to 0.8 m/s, further reflect this delta outflow. A key difference during ebb tide is the extremely weak offshore bottom currents, measuring less than 0.1 m/s. Additionally, the eastern part of the study area experiences high current velocities during ebb tide.

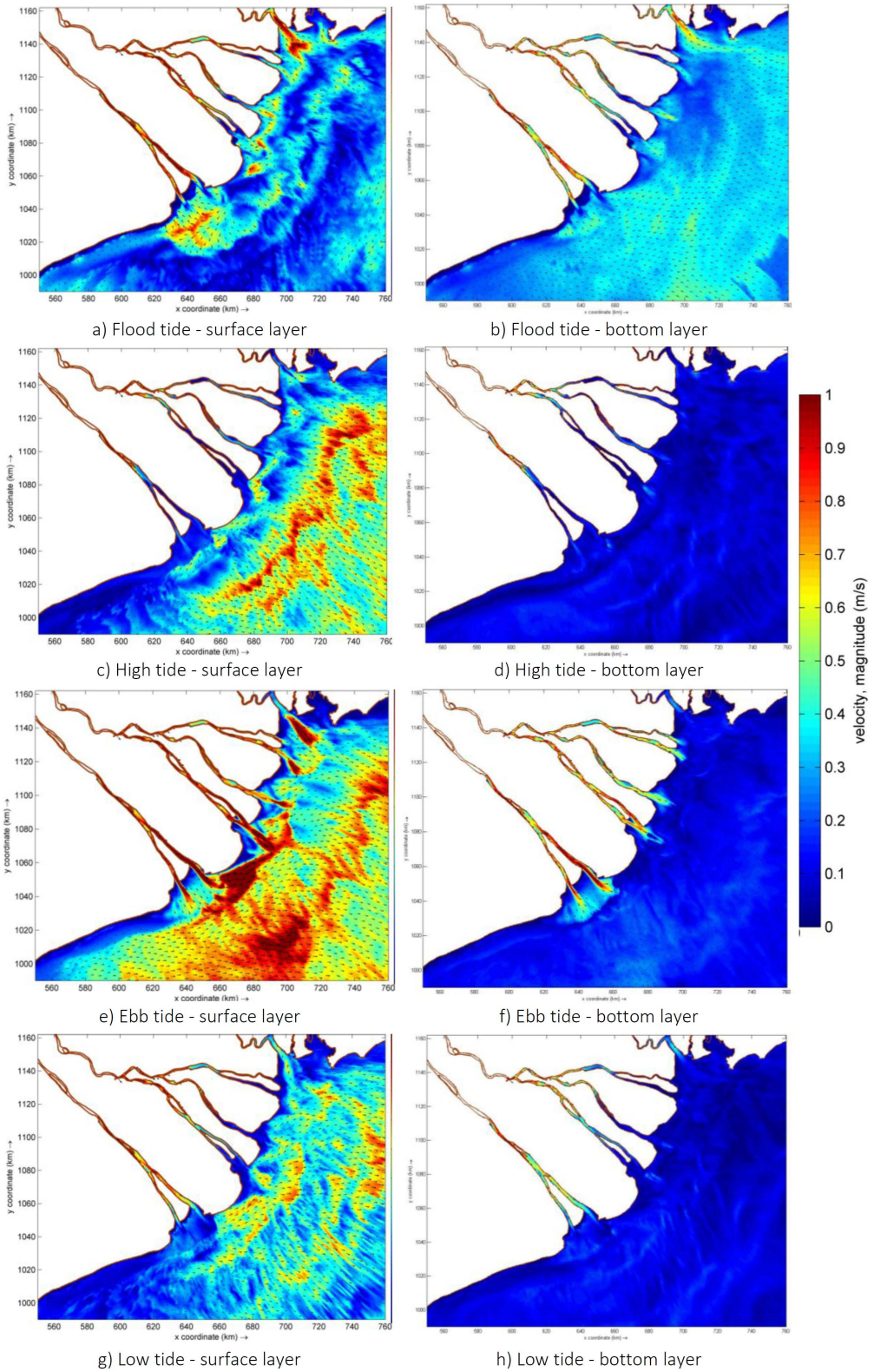

a) Flood tide - surface layer

b) Flood tide - bottom layer

c) High tide - surface layer

d) High tide - bottom layer

e) Ebb tide - surface layer

f) Ebb tide - bottom layer

g) Low tide - surface layer

h) Low tide - bottom layer

Figure 7. Current velocity (m/s) during the spring tide in July 2019

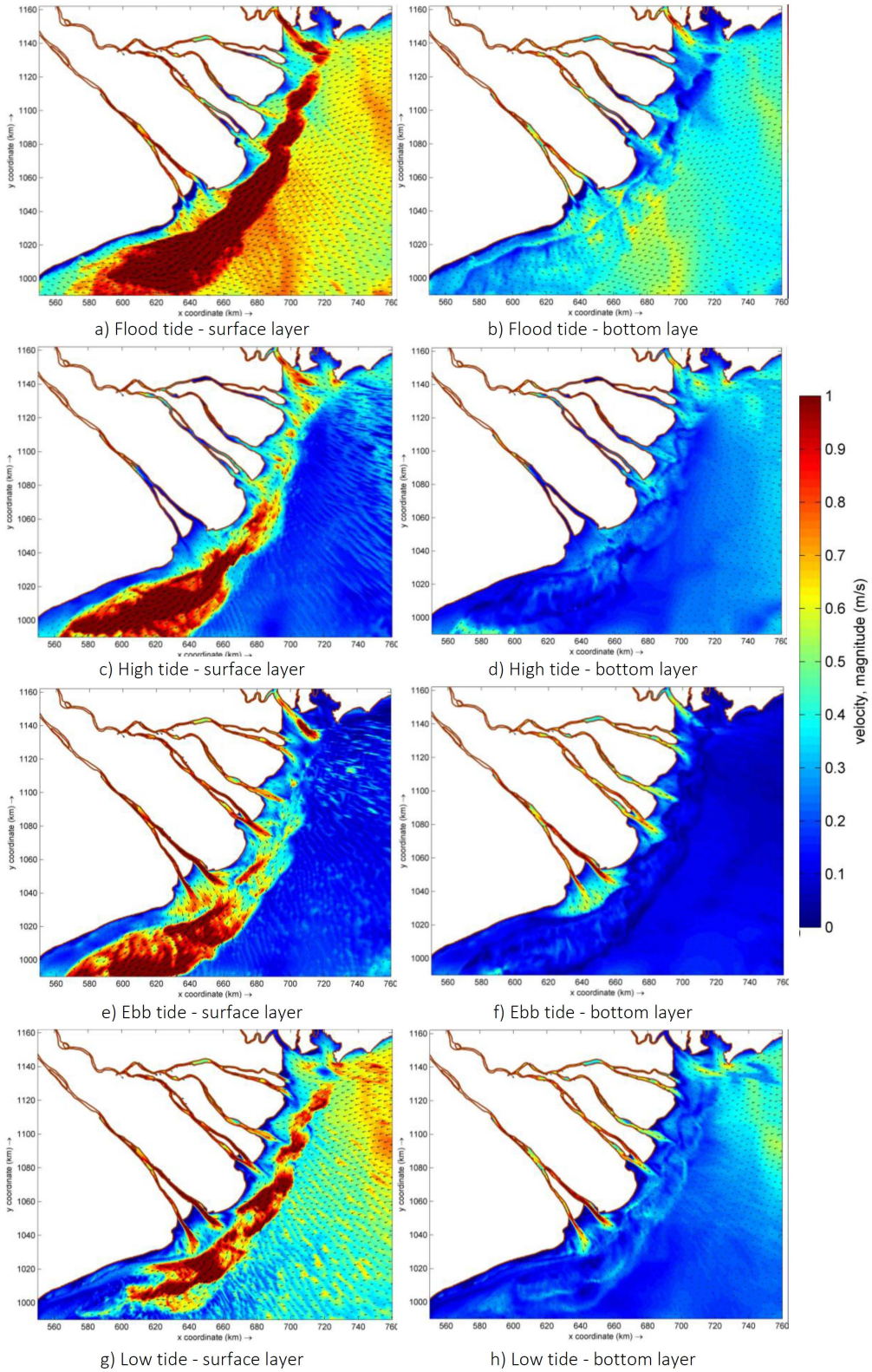

Figure 8. Current velocity (m/s) during the spring tide in October 2019

Discussion

On a seasonal scale, water levels in the MDR generally decrease during the wet season, reaching their lowest points in June/July, which coincides with the period of greatest tidal range. Conversely, water levels rise during the dry season, peaking on flood season, especially in November/December. However, this peak does not coincide with the lowest tidal ranges, which occur later, from February to March [26, 27].

Currents in the Mekong coastal area are influenced by tide, wind, and river flow, with wind and river discharge varying seasonally [13, 28, 29]. During ebb tide, flow generally directs from estuaries towards the coastal zone and from northeast to southwest, peaking in estuary areas (due to river flow intensification) and the Bac Lieu-Ca Mau coastal area. Conversely, flood tide flow typically moves from offshore towards estuaries and from southwest to northeast, also exhibiting high velocities in the Bac Lieu-Ca Mau region. At high and low tides, the interplay between wind-driven and river-driven currents complicates the integrated flow. While strong tidal currents tend to dominate the integrated current's characteristics, stronger wind or river flows can alter the current vector field, as observed in July when southwest winds shifted the surface layer integrated current vector accordingly, even during ebb tide [3, 30, 31]. Furthermore, opposing interactions between tidal currents and wind/river currents create flow convergence (flood tide) or divergence (ebb tide) regions in the Bac Lieu coastal area, occurring in both low and flood seasons, and sometimes during both ebb and flood tides. These convergence/divergence phenomena may contribute to intensified erosion in the Ganh Hai-Dam Doi coastal zone between Bac Lieu and Ca Mau Provinces.

Analysis of monthly flow velocities in the Mekong coastal zone reveals distinct seasonal patterns driven by the interplay of wind-driven currents and freshwater discharge. During the low flow season, surface layer flows are strongest, reaching 1 m/s, particularly in the coastal areas of Dinh An, Soc Trang, Bac Lieu, and Ca Mau. These flows exhibit a consistent northeast to southwest direction, mirroring the dominant northeasterly winter winds, and demonstrate minimal variation throughout January, indicating stable wind and flow direction [3, 28–31]. A gradual decrease in flow magnitude with depth (from 0.4–1 m/s at the surface to 0.05–0.6 m/s at bottom layer) suggests low stratification. In contrast, the flood season is characterized by greater regional variation in both flow velocity and direction due to the interaction of strong freshwater input and fluctuating wind patterns. While surface velocities in the Mekong estuary reach 1 m/s in October, they decrease sharply with depth, becoming very small (below 0.2 m/s at bottom layer), signifying strong stratification, unlike the low stratification observed in January. Flow directions also shift dynamically throughout the flood season: initially from southwest to northeast in early September under the influence of the Southwest monsoon, then shifting offshore (southeast) in late September as the wind weakens, followed by a southward direction in early October, and finally southwestward in late October as northeasterly winds develop and reinforce the freshwater flow from the estuary towards the Ca Mau coast. These observations highlight the dominant role of wind in driving flow during the low flow season, while freshwater discharge is the primary driver of current in the flood season, although these currents remain highly sensitive to wind direction changes as in previous studies [32–34].

Several studies [35–40] exported that sea level rise (SLR) impacts current speed distribution. In MRD, as SLR increases, average current speeds generally decrease in river channels, navigation channels outside estuaries, and offshore areas. The most significant decrease occurs in navigation channels outside estuaries. Conversely, average current speeds slightly increase in estuarine areas due to increased water influx from the sea. This increase is attributed to a decrease in the wetted cross-section of the estuaries. The magnitude of these changes becomes more pronounced with higher levels of SLR. It also shows that combining SLR with reduced upstream discharge significantly alters flow velocity. Tuan et al. [41] proved that from 14 cm

SLR and reduced discharge, river current speeds decrease sharply compared to the baseline, while offshore and navigation channel speeds change minimally.

Both the Red River and the Mekong River exhibit dynamic current patterns influenced by tides, river discharge, and monsoon winds. However, there are notable distinctions.

The Red River displays a greater diversity in surface current directions, particularly during the dry season [28, 42, 43]. In contrast, the Mekong's surface currents are more consistently directed southwestward, reflecting the dominant outflow from its delta. Regarding current velocities, both rivers experience peak speeds exceeding 1 m/s in narrow channels and near coastal areas. However, the Red River shows more pronounced spatial variations in velocity, with localized higher speeds west and northeast of Cat Ba Island during certain periods [42]. The Mekong generally maintains strong currents throughout the water column, especially near the coast, while offshore currents are comparatively weaker.

Tides play a significant role in both river systems, but their influence varies spatially and temporally. In the Red River, tidal currents are dominant during the dry season, interacting with riverine influences [35, 44]. The Mekong also experiences strong tidal currents, but they are more pronounced during the wet season and in the delta region [4]. Interestingly, the ebb tide's influence in the Red River seems primarily confined to the surface and near-coastal regions, with minimal impact on deeper offshore waters.

Both rivers exhibit distinct seasonality in their hydrodynamic regimes, driven by the monsoon climate. During the wet season, both experience increased rainfall and river discharge, leading to higher water levels and stronger currents. However, the Mekong's response to the wet season appears more prolonged, with a longer period of high-water levels compared to the Red River [42]. The transition between the Northeast and Southwest monsoons brings notable changes. The Red River's currents shift from offshore to onshore, converging towards coastal areas and estuaries. In contrast, the Mekong's currents begin to reverse, flowing from the estuary and nearshore areas towards the offshore regions [3, 44, 45].

These rivers display vertical stratification in their current profiles, but the degree of stratification varies. The Red River generally exhibits a more pronounced decrease in velocity from surface to bottom, particularly during the dry season and outside estuaries [9, 28]. The Mekong shows less distinct stratification near the coast, with strong currents throughout the water column. However, a significant stratification occurs offshore, with strong surface currents and weak bottom currents [3, 6, 8].

Conclusion

A Delft3D model effectively simulated currents in the Mekong River Delta (MRD) during 2019. The model validation demonstrated a strong agreement with measured data: water levels at Vung Tau exhibited high Nash-Sutcliffe Efficiency (*NSE*) values (0.834–0.976) and low Root Mean Square Error (*RMSE*) values (0.126–0.331), while current velocities at Ganh Hao achieved an *NSE* of 0.722 and an *RMSE* of 0.054.

The MRD's hydrodynamics are characterized by a complex interplay of tides, wind, and river flow, driving a predominantly west/southwest to east/northeast current pattern with peak speeds of 1 m/s. Seasonal variations, influenced by these factors, result in distinct ebb and flood tide flow patterns, with peak velocities in estuaries and the Bac Lieu-Ca Mau area. Wind and river flow significantly modulate these tidal currents, creating convergence/divergence zones, particularly in the Bac Lieu coastal area, impacting erosion.

Seasonal flow velocities reflect this complexity. Strong and consistent northeast-southwest flows occur during the low flow season, driven by northeasterly winds, while the flood season exhibits greater regional variability due to increased freshwater input and fluctuating winds. Projected SLR is expected to generally decrease current speeds in channels and offshore areas, while slightly increasing them in estuaries.

Acknowledgements: This study is benefited from the support of the project VAST05.04/23–24 "The study applied the method of the Empirical Mode Decomposition (EMD) to quantitatively assess the impact of sea level rise due to climate change and the ENSO phenomenon on flooding in Ho Chi Minh City".

References

[1] H. Hein, B. Hein, and T. Pohlmann, "Recent sediment dynamics in the region of Mekong water influence," *Global and Planetary Change*, vol. 110, pp. 183–194, 2013. DOI: 10.1016/j.gloplacha.2013.09.008.

[2] N. M. Nguyet, V. D. Duong, D. T. Le, L. D. Tu, C. D. San, P. N. Truong, N. Quyen, T. Bang, D. P. Wright, A. H. Tanim, and D. T. Anh, "Wave efficiency for three classes of breakwaters on the coastal Mekong Delta," *Applied Ocean Research*, vol. 129, 103362, 2022. DOI: 10.1016/j.apor.2022.103362.

[3] V. D. Vinh, S. Ouillon, N. Van Thao, and N. N. Tien, "Numerical simulations of suspended sediment dynamics due to seasonal forcing in the Mekong coastal area," *Water*, vol. 8, 255, 2016. DOI: 10.3390/w8060255.

[4] V. D. Vinh, S. Ouillon, T. D. Thanh, and C. V. Chu, "Impact of the Hoa Binh dam (Vietnam) on water and sediment budgets in the Red River basin and delta," *Hydrology and Earth System Sciences*, vol. 18, pp. 3987–4005, 2014. DOI: 10.5194/hess-18-3987-2014.

[5] T. Q. Tuan and M. T. Luan, "Monsoon wave transmission at bamboo fences protecting mangroves in the lower Mekong Delta," *Applied Ocean Research*, vol. 101, 102259, 2020. DOI: 10.1016/j.apor.2020.102259.

[6] D. Unverricht, T. C. Nguyen, C. Heinrich, W. Szczuciński, N. Lahajnar, and K. Stattegger, "Suspended sediment dynamics during the inter-monsoon season in the subaqueous Mekong Delta and adjacent shelf, southern Vietnam," *Journal of Asian Earth Sciences*, vol. 79, pp. 509–519, 2014. DOI: 10.1016/j.jseaes.2012.10.008.

[7] T. D. Dang, T. A. Cochrane, and M. E. Arias, "Quantifying suspended sediment dynamics in mega deltas using remote sensing data: A case study of the Mekong floodplains," *International Journal of Applied Earth Observation and Geoinformation*, vol. 68, pp. 105–115, 2018. DOI: 10.1016/j.jag.2018.02.008.

[8] N. N. Tien, "The influence of hydrodynamic factors on characteristics of suspended sediment distribution in the Mekong River Mouth Area," *Vietnam Journal of Marine Science and Technology*, vol. 15, pp. 150–158, 2015. DOI: 10.15625/1859-3097/15/2/6503.

[9] N. Taniguchi, C. F. Huang, M. Arai, and B. M. Howe, "Variation of residual current in the Seto Inland Sea driven by sea level difference between the Bungo and Kii Channels," *Journal of Geophysical Research: Oceans*, vol. 123, pp. 2921–2933, 2018. DOI: 10.1029/2017JC013618.

[10] T. T. N. Nguyen, D. S. Shih, L. Chua, H. N. Kieu, L. H. Ha, L. H. Nguyen, N. V. Luu, T. V. Huynh, L. M. Duong, and A. T. Ngo, "Identifying flow eddy currents in the river system as the riverbank scouring cause: A case study of the Mekong River," *Water*, vol. 14, 2022. DOI: 10.3390/w14152418.

[11] T. D. Dang, T. A. Cochrane, M. E. Arias, P. D. T. Van, and T. T. de Vries, "Hydrological alterations from water infrastructure development in the Mekong floodplains," *Hydrological Processes*, vol. 30, pp. 3824–3838, 2016. DOI: 10.1002/hyp.10894.

[12] C. A. Nittrouer, D. J. DeMaster, E. F. Eidam, T. T. Nguyen, J. P. Liu, A. S. Ogston, and P. V. Phung, "The Mekong continental shelf: The primary sink for deltaic sediment particles and their passengers," *Oceanography*, vol. 30, no. 3, pp. 60–70, 2017. DOI: 10.5670/oceanog.2017.314.

[13] A. Snidvongs and S. K. Teng, *Global International Waters Assessment, Mekong River*, GIWA Regional Assessment 55. Kalmar, Sweden: University of Kalmar, 2006.

[14] X. X. Lu and R. Y. Siew, "Water discharge and sediment flux changes over the past decades in the Lower Mekong River: possible impacts of the Chinese dams," *Hydrology and Earth System Sciences*, vol. 10, pp. 181–195, 2006. DOI: 10.5194/hess-10-181-2006.

[15] R. Costanza, R. de Groot, P. Sutton, S. Costanza, S. van der Ploeg, S. J. Anderson, I. Kubiszewski, S. Farber, and R. K. Turner, "Changes in the global value of ecosystem services," *Global*

Environmental Change, vol. 26, pp. 152–158, 2014. DOI: 10.1016/j.gloenvcha.2014.04.002.

[16] G. P. Allen, J. C. Salomon, P. Bassoullet, Y. Du Penhoat, and C. Grandpré, "Effects of tides on mixing and suspended sediment transport in macrotidal estuaries," *Sedimentary Geology*, vol. 26, pp. 69–90, 1980. DOI: 10.1016/0037-0738(80)90006-8.

[17] E. Wolanski, N. N. Huan, L. T. Dao, N. H. Nhan, and N. N. Thuy, "Fine-sediment dynamics in the Mekong River estuary, Vietnam," *Estuarine, Coastal and Shelf Science*, vol. 43, pp. 565–582, 1996. DOI: 10.1006/ecss.1996.0088.

[18] A. Sottolichio, P. Le Hir, and P. Castaing, "Modeling mechanisms for the stability of the turbidity maximum in the Gironde estuary, France," *Proceedings in Marine Science*, vol. 2–3, pp. 373–386, 2000. DOI: 10.1016/S1568-2692(00)80132-1.

[19] H. Loisel, A. Mangin, V. Vantrepotte, D. Dessailly, D. D. Ngoc, P. Garnesson, S. Ouillon, J. P. Lefebvre, X. Mériaux, and P. M. Thu, "Variability of suspended particulate matter concentration in coastal waters under the Mekong's influence from ocean color (MERIS) remote sensing over the last decade," *Remote Sensing of Environment*, vol. 150, pp. 218–230, 2014. DOI: 10.1016/j.rse.2014.05.006.

[20] A. S. Ogston, M. A. Allison, R. L. McLachlan, D. J. Nowacki, and J. D. Stephens, "How tidal processes impact the transfer of sediment from source to sink: Mekong River collaborative studies," *Oceanography*, vol. 30, no. 3, pp. 22–33, 2017. DOI: 10.5670/oceanog.2017.311.

[21] P. Weatherall, K. M. Marks, M. Jakobsson, T. Schmitt, S. Tani, J. E. Arndt, M. Rovere, D. Chayes, V. Ferrini, and R. Wigley, "A new digital bathymetric model of the world's oceans," *Earth and Space Science*, vol. 2, no. 8, pp. 331–345, 2015. DOI: 10.1002/2015EA000107.

[22] Delft Hydraulics, *Delft3D-FLOW User Manual*, 2003.

[23] J. A. Battjes and J. P. F. M. Janssen, "Energy loss and set-up due to breaking of random waves," in *Coastal Engineering 1978*, pp. 569–587, 1978. doi: 10.1061/9780872621909.034.

[24] J. E. Nash and J. V. Sutcliffe, "River flow forecasting through conceptual models part I—A discussion of principles," *Journal of Hydrology*, vol. 10, no. 3, pp. 282–290, 1970. DOI: 10.1016/0022-1694(70)90255-6.

[25] R. L. Sapra, "Using R^2 with caution," *Current Medicine Research and Practice*, vol. 4, no. 3, pp. 130–134, 2014. DOI: 10.1016/j.cmrp.2014.06.002.

[26] T. C. Nguyen, K. Schwarzer, and K. Ricklefs, "Water-level changes and subsidence rates along the Saigon-Dong Nai River Estuary and the East Sea coastline of the Mekong Delta," *Estuarine, Coastal and Shelf Science*, vol. 283, 108259, 2023. DOI: 10.1016/j.ecss.2023.108259.

[27] A. V. Vu, L. J. Baumgartner, G. S. Doran, M. Mallen-Cooper, J. D. Thiem, J. A. Howitt, K. E. Limburg, B. M. Gillanders, and I. G. Cowx, "Variability in water chemistry in the Lower Mekong Basin: considerations for fish life history reconstruction," *Estuarine, Coastal and Shelf Science*, vol. 255, 107355, 2021. DOI: 10.1016/j.ecss.2021.107355.

[28] H. M. Nguyen, S. Ouillon, and V. D. Vu, "Sea level variation and trend analysis by comparing Mann–Kendall test and innovative trend analysis in front of the Red River Delta, Vietnam (1961–2020)," *Water*, vol. 14, no. 11, 1709, 2022. DOI: 10.3390/w14111709.

[29] Z. Xue, J. P. Liu, and Q. Ge, "Changes in hydrology and sediment delivery of the Mekong River in the last 50 years: connection to damming, monsoon, and ENSO," *Earth Surface Processes and Landforms*, vol. 36, no. 3, pp. 296–308, 2011. DOI: 10.1002/esp.2036.

[30] P. S. Hoan and N. K. Vinh, "Current characteristics in the waters of Khanh Hoa Province during Southwest monsoon period," *Vietnam Journal of Marine Science and Technology*, vol. 12, no. 3, pp. 57–66, 2012. DOI: 10.15625/1859-3097/12/3/2374.

[31] C. Chen, Z. Lai, R. C. Beardsley, Q. Xu, H. Lin, and N. T. Viet, "Current separation and upwelling over the southeast shelf of Vietnam in the South China Sea," *Journal of Geophysical Research: Oceans*, vol. 117, no. C3, 2012. DOI: 10.1029/2011JC007150.

[32] A. M. Maxam and D. F. Webber, "The influence of wind-driven currents on the circulation and bay dynamics of a semi-enclosed reefal bay, Wreck Bay, Jamaica," *Estuarine, Coastal and*

Shelf Science, vol. 87, no. 4, pp. 535–544, 2010. DOI: 10.1016/j.ecss.2010.02.007.

[33] A. Jalil, Y. Li, W. Du, W. Wang, J. Wang, X. Gao, H. O. S. Khan, B. Pan, and K. Acharya, "The role of wind field induced flow velocities in destratification and hypoxia reduction at Meiling Bay of large shallow Lake Taihu, China," *Environmental Pollution*, vol. 232, pp. 591–602, 2018. DOI: 10.1016/j.envpol.2017.09.095.

[34] J. Yang and K. Chen, "The role of wind stress in driving the along-shelf flow in the northwest Atlantic Ocean," *Journal of Geophysical Research: Oceans*, vol. 126, no. 4, 2021, e2020JC016757. DOI: 10.1029/2020JC016757.

[35] N. M. Hai, V. D. Vinh, and T. D. Lan, "Impact of sea level rise on current and wave in Van Uc coastal area," *Vietnam Journal of Marine Science and Technology*, vol. 19, no. 3, pp. 313–325, 2019. DOI: 10.15625/1859-3097/19/3/13928.

[36] M. Yahya Surya, Z. He, Y. Xia, and L. Li, "Impacts of sea level rise and river discharge on the hydrodynamics characteristics of Jakarta Bay (Indonesia)," *Water*, vol. 11, no. 7, 1384, 2019. DOI: 10.3390/w11071384.

[37] D. Khojasteh, W. Glamore, V. Heimhuber, and S. Felder, "Sea level rise impacts on estuarine dynamics: A review," *Science of The Total Environment*, vol. 780, 146470, 2021. DOI: 10.1016/j.scitotenv.2021.146470.

[38] J. M. Valentim, L. Vaz, N. Vaz, H. Silva, B. Duarte, I. Caçador, and J. M. Dias, "Sea level rise impact in residual circulation in Tagus estuary and Ria de Aveiro lagoon," *Journal of Coastal Research*, vol. 65, no. SI, pp. 1981–1986, 2013. DOI: 10.2112/SI65-335.1.

[39] C. L. Lopes and J. M. Dias, "Tidal dynamics in a changing lagoon: Flooding or not flooding the marginal regions," *Estuarine, Coastal and Shelf Science*, vol. 167, pp. 14–24, 2015. DOI: 10.1016/j.ecss.2015.05.043.

[40] A. R. Carrasco, T. Plomaritis, J. Reyns, Ó. Ferreira, and D. Roelvink, "Tide circulation patterns in a coastal lagoon under sea-level rise," *Ocean Dynamics*, vol. 68, no. 9, pp. 1121–1139, 2018. DOI: 10.1007/s10236-018-1178-0.

[41] M. T. Vu, C. Luu, D. Q. Bui, Q. H. Vu, and M. Q. Pham, "Simulation of hydrodynamic changes and salinity intrusion in the lower Vietnamese Mekong Delta under climate change-induced sea level rise and upstream river discharge," *Regional Studies in Marine Science*, vol. 78, 103749, 2024. DOI: 10.1016/j.rsma.2024.103749.

[42] V. D. Vinh, N. M. Hai, S. P. Purayil, G. Lacroix, and N. T. Duong, "Seasonal variation of coastal currents and residual currents in the CAT BA–HA long coastal area (VIET NAM): Results of coherens model," *Regional Studies in Marine Science*, vol. 80, 103874, 2024. DOI: 10.1016/j.rsma.2024.103874.

[43] V. D. Vinh and T. D. Thanh, "Characteristics of current variation in the coastal area of Red River Delta—results of research using the 3D numerical model," *Vietnam Journal of Marine Science and Technology*, vol. 14, no. 2, pp. 139–148, 2014. DOI: 10.15625/1859-3097/14/2/4480.

[44] J. P. Lefebvre, S. Ouillon, V. D. Vinh, R. Arfi, J. Y. Panché, X. Mari, C. V. Thuoc, and J. P. Torréton, "Seasonal variability of cohesive sediment aggregation in the Bach Dang–Cam Estuary, Haiphong (Vietnam)," *Geo-Marine Letters*, vol. 32, no. 2, pp. 103–121, 2012. DOI: 10.1007/s00367-011-0273-8.

[45] V. D. Vinh and S. Ouillon, "The double structure of the estuarine turbidity maximum in the Cam–Nam Trieu mesotidal tropical estuary, Vietnam," *Marine Geology*, vol. 442, 106670, 2021. DOI: 10.1016/j.margeo.2021.106670.